Available online at www.eccomasproceedia.org
Eccomas Proceedia SMART (2023) 303-316

ECCOMAS
Proceedia

X ECCOMAS Thematic Conference on Smart Structures and Materials
SMART 2023
D.A. Saravanos, A. Benjeddou, N. Chrysochoidis and T. Theodosiou (Eds)

MULTI-PHYSICS MODELING OF INDUCED-STRAIN ACTUATED WINGS FOR MECHANISM-FREE ORNITHOPTERS

XIN SHAN* **AND ONUR BILGEN†**

* Department of Mechanical and Aerospace Engineering
Rutgers University
98 Brett Road, Piscataway, New Jersey, 08854, USA
e-mail: xin.shan@rutgers.edu, www.rutgers.edu

† Department of Mechanical and Aerospace Engineering
Rutgers University
98 Brett Road, Piscataway, New Jersey, 08854, USA
e-mail: o.bilgen@rutgers.edu, www.rutgers.edu

Abstract. Induced-strain actuators, for example piezoelectric and electro-active polymer devices, can be bonded to elastic substrates to induce flapping-like motion to form synthetic wings. Ornithopters equipped with induced-strain actuated wings do not need conventional motors and mechanisms (i.e., revolute and prismatic), potentially saving weight and energy consumption, reducing mechanical complexity, and improving wing durability. By optimizing actuator placements, excitation amplitude and phase, substrate thickness/stiffness distribution, wing mounting position, etc., a mechanism-free wing may be able to reproduce features of natural flyers. In this research, a multi-physics strongly-coupled lumped parameter model is developed to predict the dynamic response of a mechanism-free wing, which is then used in ornithopter design and controller optimization, also termed control co-design. The modeling of an induced-strain actuated ornithopter wing involves modeling of fluid-structure interaction and circuit-actuator electromechanical coupling. The structural model of the composite wing with a customizable profile is based on the Rayleigh-Ritz method. The fluid-induced effects on the wings have several contributions such as added mass and damping, and quasi-steady and unsteady aerodynamic forces. The wing, fluid-induced effects, and circuit are integrated to derive the lumped parameter governing equations using Hamilton's principle. Since the structure, fluid, and circuit domains being all represented by the lumped-parameter sub-systems, the coupling between different domains is clearly defined and exposed. The reduced-order model proposed in this paper is computationally efficient, suitable for trade studies and multi-disciplinary design optimization, and can be easily converted to state representation for controller development purposes.

Key words: Induced-strain Actuation, Flapping Wing, Electromechanical Coupling, Rayleigh-Ritz Method, Fluid-structure Interaction.

Peer-review under responsibility of the organizing committee of SMART 2023.
doi: 10.7712/150123.9787.443787

1 INTRODUCTION

Flapping based flight has high aerodynamic efficiency that can be twice that of rotatory propulsion in low Reynolds number conditions, and is nearly silent compared to rotary propulsion [1-3]. Existing flapping ornithopters, especially miniature-sized flapping air vehicles ($10\ \text{g} - 100\ \text{g}$ weight), almost all use mechanisms, joints, and hinges to convert the rotational motion produced by electromagnetic motors to the rectilinear flapping motion of the passive wings [4-10]. Natural fliers, such as hummingbirds and insects, show complex plunge and pitch patterns in wing strokes, exhibiting sophisticated wing kinematic features including pronation, supination, clapping, and fling [11]. Passive wings driven by mechanisms with finite degrees of freedom cannot reproduce the wing kinematics of natural flapping flight seen in avians. The failure to properly reproduce natural wing kinematics leads to synthetic flapping flight to significantly underperform in maneuverability, range, endurance, etc. In contrast, induced-strain actuated wings installed on a so-called solid-state (i.e., mechanism-free) ornithopter are capable of active morphing, high frequency actuation, and complex shape control by various design variables such as actuator placement, substrate stiffness distribution, and operational variables such as excitation amplitude, frequency, phase difference, etc. [3, 12-14].

The application of piezoelectric material based induced-strain actuators has been reported in insect-scale micro air vehicles (MAVs), approximately $20\ \text{cm}$ or less in dimension and $20\ \text{g}$ or less in weight. This scale leads to a low Reynolds number regime, increasing the contribution of viscous effects whereas decreasing the inertial contribution of the wing. To compensate, a higher flapping rate is required, usually hundreds of Hertz [15, 16], which is suitable for piezoelectric material devices. Smart composite microstructures (SCM) technology [17-19], developed at the University of California, Berkley, was used in a piezoelectric actuated flapping flight. Nogar, et al. [20] developed a computationally efficient electromechanical-aeroelastic nonlinear model with passive wings. The implicit condensation technique based on the finite element method (FEM) [21, 22] was used to represent the wing's large amplitude nonlinear deformations in the coupled lumped-parameter model. The aerodynamic loads were represented using the Duhamel's principle [11]. In the MAV designs mentioned above, wings were all actuated with the help of mechanisms to achieve certain kinematics. Guo, et al. [23] were partially able to eliminate mechanisms in actuation. The wings were actuated by a unimorph THUNDER actuator. A twisting motion was resulted due to the asymmetry of the wing structure. The wing surface was made of passive films without the capability of active morphing.

1.1 Contributions

In this research, the Macro-Fiber Composite (MFC) piezocomposite device is selected as the induced-strain actuator. The MFC, invented by NASA Langley Research Center [24, 25], is a piezoelectric-based induced-strain actuator with structural flexibility and relatively high strain actuation authority, outperforming monolithic piezoceramic devices [26, 27].

A major challenge in the design of a mechanism-free ornithopter is the dynamic complexity and lack of accurate and computationally efficient models for design and control optimization.

The CFD and FEM approaches are computationally expensive and thus not suitable for the ornithopter design optimization and real-time control, where intensive parameter studies or low delay are required. In this paper, based on the authors' previous work [1, 14, 28-33], a multi-physics strongly-coupled lumped parameter model is presented to predict the dynamic behavior of the mechanism-free ornithopter. The Rayleigh-Ritz method incorporating the in-plane extensions is used in the wing structural modeling to account for large amplitude flapping and customizable wing profile. The fluid effects are represented by: (1) the added mass and damping, (2) the steady aerodynamic forces calculated by a vortex lattice method, and (3) the unsteady aerodynamic forces calculated by the extended Theodorsen formulation.

1.2 Outline

The rest of the paper is organized as follows. First, the conceptual model of the proposed mechanism-free ornithopter is introduced. Next, the mechanical, fluid, and piezoelectric domains are modeled successively. Based on the strongly-coupled multi-physics model, and the simulations are conducted to investigate MFC placement, driving voltage frequencies, etc. The conclusions are drawn at the end.

2 CONCEPTUAL MODEL OF THE MECHANISM-FREE ORNITHOPTER

Figure 1 (**a**) and (**b**) show a system conceptual model and a representative diagram of the system respectively. The ornithopter model is composed of two piezocomposite flapping wings, a rigid ornithopter body which includes the tail, and the driving circuit. The wing and tail positions from the center of mass are $\{d_x^W, d_y^W\}$ and $\{d_x^T, d_y^T\}$ respectively. For simplicity, the ornithopter body is considered fixed in this work. The body-wing interaction is not investigated.

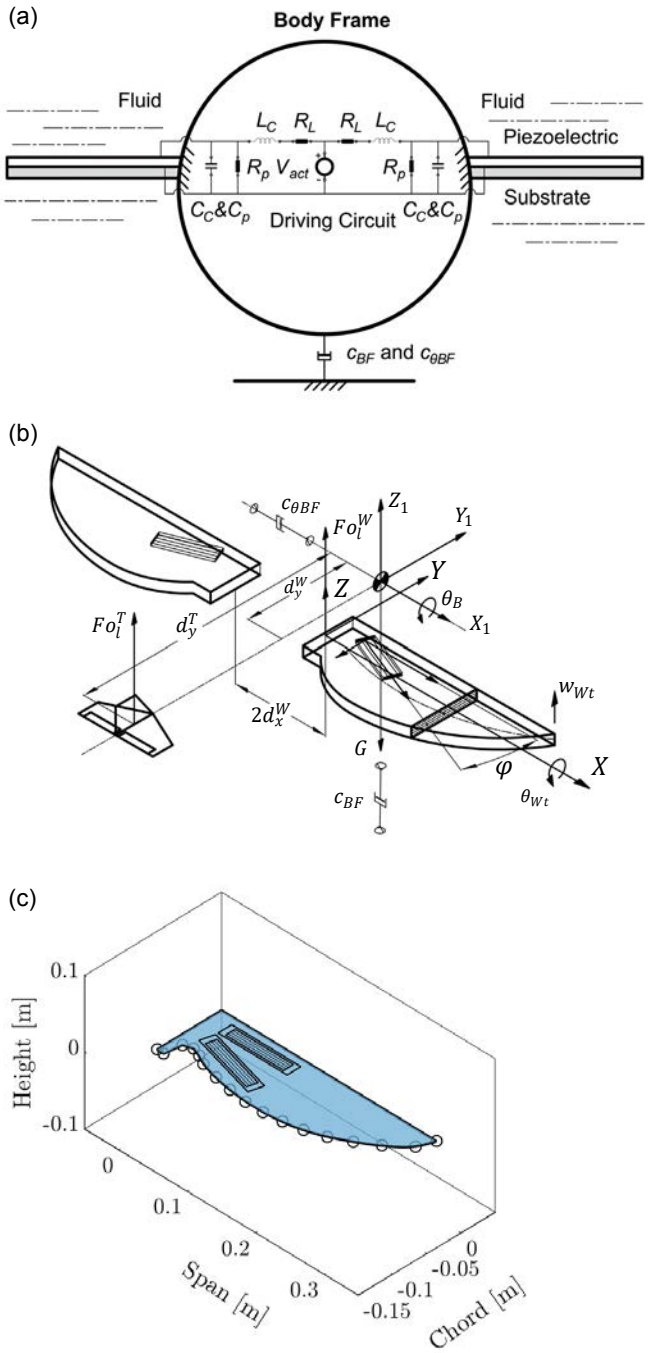

Figure 1: System and wing diagrams. (**a**) System conceptual model. (**b**) Free body diagram of the ornithopter. (**c**) Wing shape characterization.

The wing trailing edge profile is a spline curve customizable by setting up the control points in **Figure 1** (**c**). Each MFC actuator is actuated independently. The placement of each MFC

actuator is described by the root coordinates and orientation, i.e., $\{x_{MFC,i}, y_{MFC,i}, \varphi_{MFC,i}\}$ where the subscripts denote the number of the MFC actuator.

3 MODELING OF THE ORNITHOPTER WING

Multiple MFC actuators are assumed to be mounted on the top surface of a wing-shaped substrate, yielding a unimorph configuration. In-plane extensions [34] are considered in the Rayleigh-Ritz method to account for large amplitude deformation. The constitutive equations of different wing layers are presented. Based on the constitutive equations, using the Rayleigh-Ritz method, the mass, damping, and stiffness matrices are derived from the energy formulations of the system. The distributed flapping-induced inertial and viscous forces are represented by added mass and damping acting on the wing cross-section. The Athena Vortex Lattice (AVL) program, based on an extended vortex lattice method, is used to obtain steady aerodynamic coefficients and stability derivatives. The unsteady aerodynamic forces are calculated by the Theodorsen formulation [35].

3.1 Mechanical Domain

In the Rayleigh-Ritz approach [36], the displacement fields in the X, Y and Z directions are given by:

$$\{\boldsymbol{u}\} = \begin{Bmatrix} u \\ v \\ w \end{Bmatrix} = \sum_{i=1}^{M}\sum_{j=1}^{N} \begin{Bmatrix} \psi_{ij}^{u}(x,y) q_{ij}^{u}(t) \\ \psi_{ij}^{v}(x,y) q_{ij}^{v}(t) \\ \psi_{ij}^{w}(x,y) q_{ij}^{w}(t) \end{Bmatrix} = \sum_{i=1}^{5}\sum_{j=1}^{6} \begin{Bmatrix} x^{i} y^{j-1} q_{ij}^{u}(t) \\ x^{i} y^{j-1} q_{ij}^{v}(t) \\ x^{i+1} y^{j-1} q_{ij}^{w}(t) \end{Bmatrix}, \tag{1}$$

where $\psi_{ij}^{u}(x,y), \psi_{ij}^{v}(x,y),$ and $\psi_{ij}^{u}(x,y)$ are the polynomial assumed shapes of the displacements in the X, Y and Z directions, and $q_{ij}^{u}(t), q_{ij}^{v}(t),$ and $q_{ij}^{w}(t)$ are the corresponding generalized coordinates. The clamped boundary condition at $x = 0$ is satisfied by the assumed shapes. The displacement fields can be written in the matrix production form:

$$\{\boldsymbol{u}\} = \begin{Bmatrix} \boldsymbol{\psi}_{\boldsymbol{u}}^{\boldsymbol{T}} \boldsymbol{q}_{\boldsymbol{u}} \\ \boldsymbol{\psi}_{\boldsymbol{v}}^{\boldsymbol{T}} \boldsymbol{q}_{\boldsymbol{v}} \\ \boldsymbol{\psi}_{\boldsymbol{w}}^{\boldsymbol{T}} \boldsymbol{q}_{\boldsymbol{w}} \end{Bmatrix} = \begin{bmatrix} \boldsymbol{\psi}_{\boldsymbol{u}}^{\boldsymbol{T}} & \boldsymbol{0} & \boldsymbol{0} \\ \boldsymbol{0} & \boldsymbol{\psi}_{\boldsymbol{v}}^{\boldsymbol{T}} & \boldsymbol{0} \\ \boldsymbol{0} & \boldsymbol{0} & \boldsymbol{\psi}_{\boldsymbol{w}}^{\boldsymbol{T}} \end{bmatrix} \begin{Bmatrix} \boldsymbol{q}_{\boldsymbol{u}} \\ \boldsymbol{q}_{\boldsymbol{v}} \\ \boldsymbol{q}_{\boldsymbol{w}} \end{Bmatrix} = [\boldsymbol{H}]_{3\times 90} \{\boldsymbol{q}\}_{90\times 1}, \tag{2}$$

where $\{\boldsymbol{\psi}_{\boldsymbol{u}}\} = \{\psi_{11}^{u}, \psi_{12}^{u}, \dots, \psi_{MN}^{u}\}^{T}$, $\{\boldsymbol{\psi}_{\boldsymbol{v}}\} = \{\psi_{11}^{v}, \psi_{12}^{v}, \dots, \psi_{MN}^{v}\}^{T}$, and $\{\boldsymbol{\psi}_{\boldsymbol{w}}\} = \{\psi_{11}^{w}, \psi_{12}^{w}, \dots, \psi_{MN}^{w}\}^{T}$ are the assumed shape vectors, and $\{\boldsymbol{q}_{\boldsymbol{u}}\} = \{q_{11}^{u}, q_{12}^{u}, \dots, q_{MN}^{u}\}^{T}$, $\{\boldsymbol{q}_{\boldsymbol{v}}\} = \{q_{11}^{v}, q_{12}^{v}, \dots, q_{MN}^{v}\}^{T}$, and $\{\boldsymbol{q}_{\boldsymbol{w}}\} = \{q_{11}^{w}, q_{12}^{w}, \dots, q_{MN}^{w}\}^{T}$ are the generalized coordinate vectors in the X, Y and Z directions.

The piezocomposite wing is composed of a wing-like passive substrate with multiple MFC actuators bonded to it. The carbon-fiber composite and MFC actuators all exhibit orthotropic properties. The wing substrate is a two-layered 2×2 twill weave carbon-fiber composite impregnated with epoxy, which serves as the matrix material. The wing substrate is fabricated using the vacuum bagging technique [1]. The carbon-fiber weaves are placed on a flat mold,

impregnated by two-part epoxy, and held together in the vacuum bag until the epoxy is cured. A thin glue layer is formed between the carbon-fiber laminae. The wing substrate is non-uniform in thickness due to the uneven pressure and epoxy distribution in the vacuum bagging. Such thickness non-uniformity is accumulated as the layer number increases [1]. The carbon-fiber epoxy lamina and glue layer thicknesses in the modeling are taken as the mean value of the thicknesses at different wing positions, measured by Hauris [1]. Considering the strength, thickness, and bending rigidity to sustain its own weight, a two-layered carbon-fiber composite is used in the prototype.

For the passive layers, the extension forces and moments per unit width for each layer are calculated by integrating the stresses over the height, given by:

$$\begin{Bmatrix} N_x^i \\ N_y^i \\ N_{xy}^i \end{Bmatrix} = \begin{bmatrix} Q_{11}^i & Q_{12}^i & Q_{16}^i \\ Q_{12}^i & Q_{22}^i & Q_{26}^i \\ Q_{61}^i & Q_{62}^i & Q_{66}^i \end{bmatrix} \int_{z_i}^{z_{i+1}} \left[\begin{Bmatrix} \varepsilon_x^0 \\ \varepsilon_y^0 \\ \gamma_{xy}^0 \end{Bmatrix} + z \begin{Bmatrix} \kappa_x \\ \kappa_y \\ \kappa_{xy} \end{Bmatrix} \right] dz$$

$$= (z_{i+1} - z_i)[\boldsymbol{Q^i}]\{\boldsymbol{\varepsilon}\} + \frac{1}{2}(z_{i+1}^2 - z_i^2)[\boldsymbol{Q^i}]\{\boldsymbol{\kappa}\} = [\boldsymbol{A^i}]\{\boldsymbol{\varepsilon}\} + [\boldsymbol{B^i}]\{\boldsymbol{\kappa}\}, \tag{3}$$

$$\begin{Bmatrix} M_x^i \\ M_y^i \\ M_{xy}^i \end{Bmatrix} = \begin{bmatrix} Q_{11}^i & Q_{12}^i & Q_{16}^i \\ Q_{12}^i & Q_{22}^i & Q_{26}^i \\ Q_{61}^i & Q_{62}^i & Q_{66}^i \end{bmatrix} \int_{z_i}^{z_{i+1}} \left[\begin{Bmatrix} \varepsilon_x^0 \\ \varepsilon_y^0 \\ \gamma_{xy}^0 \end{Bmatrix} + z \begin{Bmatrix} \kappa_x \\ \kappa_y \\ \kappa_{xy} \end{Bmatrix} \right] z dz$$

$$= \frac{1}{2}(z_{i+1}^2 - z_i^2)[\boldsymbol{Q^i}]\{\boldsymbol{\varepsilon}\} + \frac{1}{3}(z_{i+1}^3 - z_i^3)[\boldsymbol{Q^i}]\{\boldsymbol{\kappa}\} = [\boldsymbol{B^i}]\{\boldsymbol{\varepsilon}\} + [\boldsymbol{D^i}]\{\boldsymbol{\kappa}\}.$$

The forces and moments can be written in the compact matrix form:

$$\begin{Bmatrix} \boldsymbol{N^i} \\ \boldsymbol{M^i} \end{Bmatrix} = \begin{bmatrix} \boldsymbol{A^i} & \boldsymbol{B^i} \\ \boldsymbol{B^i} & \boldsymbol{D^i} \end{bmatrix} \begin{Bmatrix} \boldsymbol{\varepsilon} \\ \boldsymbol{\kappa} \end{Bmatrix}, \tag{4}$$

where $\{\boldsymbol{N^i}\} = \{N_x^i, N_y^i, N_{xy}^i\}^T$, $\{\boldsymbol{M^i}\} = \{M_x^i, M_y^i, M_{xy}^i\}^T$, $\{\boldsymbol{\varepsilon}\} = \{\varepsilon_x, \varepsilon_y, \varepsilon_{xy}\}^T$, and $\{\boldsymbol{\kappa}\} = \{\kappa_x, \kappa_y, \kappa_{xy}\}^T$ are the force, moment, strain, and curvature vectors, respectively. The strains and curvatures can be expressed by [34]:

$$\begin{Bmatrix}\boldsymbol{\varepsilon}\\ \boldsymbol{\kappa}\end{Bmatrix}_{6\times1}=\begin{bmatrix}\frac{\partial}{\partial x} & 0 & 0\\ 0 & \frac{\partial}{\partial y} & 0\\ \frac{\partial}{\partial y} & \frac{\partial}{\partial x} & 0\\ 0 & 0 & \frac{\partial^2}{\partial x^2}\\ 0 & 0 & \frac{\partial^2}{\partial y^2}\\ 0 & 0 & \frac{\partial^2}{\partial x\partial y}\end{bmatrix}\begin{Bmatrix}u\\ v\\ w\end{Bmatrix}=[\mathfrak{D}]_{6\times3}\{\boldsymbol{u}\}_{3\times1} \tag{5}$$

where $[\mathfrak{D}]$ is the derivative operator.

The MFC actuator (i.e., MFC M8514-P1 manufactured by Smart Material Corporation, Germany) itself is a composite device composed of piezoceramic fibers adhered by epoxy matrix, sandwiched by electrode layers and protective Kapton polyimide films. The MFC actuators are glued to the substrate top surface by 3M™ DP460 two-part epoxy. The glue layer is omitted in the modeling due to its negligible thickness. For the piezoceramic layer, the extension forces and moments per unit width are calculated by:

$$\begin{Bmatrix}\boldsymbol{N}^{i=5}\\ \boldsymbol{M}^{i=5}\end{Bmatrix}=\begin{bmatrix}\boldsymbol{A^p} & \boldsymbol{B^p}\\ \boldsymbol{B^p} & \boldsymbol{D^p}\end{bmatrix}\begin{Bmatrix}\boldsymbol{\varepsilon}\\ \boldsymbol{\kappa}\end{Bmatrix}-\begin{Bmatrix}\boldsymbol{N_p}\\ \boldsymbol{M_p}\end{Bmatrix}, \tag{6}$$

where $\{\boldsymbol{N_p}\}=E_{p3}[\boldsymbol{A^p}]\{\boldsymbol{d^p}\}$ and $\{\boldsymbol{M_p}\}=E_{p3}[\boldsymbol{B^p}]\{\boldsymbol{d^p}\}$ are the generalized piezoelectric-induced force and moment vectors, respectively.

Ignoring the rotational inertia, and substituting the assumed shape matrix $[\boldsymbol{H}]$ in Equation (2), the kinetic energy of a single piezocomposite wing is given by:

$$T_W=\frac{1}{2}\sum_{i=1}^{6}\iint_{S_i}\rho_i h_i\{\dot{\boldsymbol{u}}\}^T\{\dot{\boldsymbol{u}}\}dxdy=\frac{1}{2}\{\dot{\boldsymbol{q}}\}^T\left(\sum_{i=1}^{6}\iint_{S_i}\rho_i h_i[\boldsymbol{H}]^T[\boldsymbol{H}]dxdy\right)\{\dot{\boldsymbol{q}}\}=\frac{1}{2}\{\dot{\boldsymbol{q}}\}^T[\boldsymbol{M_W}]\{\dot{\boldsymbol{q}}\}, \tag{7}$$

where the subscript $(\,)_W$ denotes the piezocomposite wing, S_i is the area function for different layers, $S_i=S_W$ for $i=1\sim3$, and $S_i=S_{MFC}$ for $=4\sim6$. The wing's mass matrix $[\boldsymbol{M_W}]$ is given by:

$$[\boldsymbol{M_W}]=\sum_{i=1}^{6}\iint_{S_i}\rho_i h_i\begin{bmatrix}\boldsymbol{\psi_u\psi_u^T} & \boldsymbol{0} & \boldsymbol{0}\\ \boldsymbol{0} & \boldsymbol{\psi_v\psi_v^T} & \boldsymbol{0}\\ \boldsymbol{0} & \boldsymbol{0} & \boldsymbol{\psi_w\psi_w^T}\end{bmatrix}dxdy. \tag{8}$$

Using the constitutive Equation (4) and (6), the strain-displacement relation in Equation (5), and the assumed shape matrix $[\boldsymbol{H}]$ in Equation (2), the strain energy of a single wing U_W is given by:

$$U_W = \frac{1}{2}\sum_{\substack{i=1\\ i\neq 5}}^{6}\iint_{S_i}\begin{Bmatrix}\boldsymbol{\varepsilon}\\ \boldsymbol{\kappa}\end{Bmatrix}^T\begin{bmatrix}\boldsymbol{A^i} & \boldsymbol{B^i}\\ \boldsymbol{B^i} & \boldsymbol{D^i}\end{bmatrix}\begin{Bmatrix}\boldsymbol{\varepsilon}\\ \boldsymbol{\kappa}\end{Bmatrix}dxdy - \iint_{S_{i=5}}\begin{Bmatrix}\boldsymbol{\varepsilon}\\ \boldsymbol{\kappa}\end{Bmatrix}^T\begin{Bmatrix}\boldsymbol{N_p}\\ \boldsymbol{M_p}\end{Bmatrix}dxdy$$

$$= \frac{1}{2}\{\boldsymbol{q}\}^T\left(\sum_{\substack{i=1\\ i\neq 5}}^{6}\iint_{S_i}[\boldsymbol{H}]^T[\mathfrak{D}]^T\begin{bmatrix}\boldsymbol{A^i} & \boldsymbol{B^i}\\ \boldsymbol{B^i} & \boldsymbol{D^i}\end{bmatrix}[\mathfrak{D}][\boldsymbol{H}]dxdy\right)\{\boldsymbol{q}\} \tag{9}$$

$$-\{\boldsymbol{q}\}^T\left(E_{\mathrm{P3}}\iint_{S_{i=5}}[\boldsymbol{H}]^T[\mathfrak{D}]^T\begin{bmatrix}\boldsymbol{A^p}\\ \boldsymbol{B^p}\end{bmatrix}\{\boldsymbol{d^p}\}dxdy\right) = \frac{1}{2}\{\boldsymbol{q}\}^T[\boldsymbol{K_W}]\{\boldsymbol{q}\} - \{\boldsymbol{q}\}^T\{\boldsymbol{F_p}\}.$$

where $[\boldsymbol{K_W}]$ is the wing's stiffness matrix, and $\{\boldsymbol{F_p}\}$ is the generalized piezoelectric equivalent force vector.

3.2 Fluid Domain

The fluid forces exerting on the ornithopter include inertial and viscosity-induced forces, and steady, unsteady aerodynamic forces. The inertial and viscosity induced forces are calculated based on the model developed and experimentally validated by Aureli, et al. [37], where the non-linear convection is accounted for. The force and torque exerted on wing cross-section per unit length f_{WF} [38] and τ_{WF} can be expressed as:

$$\begin{cases} f_{WF} = -\mathcal{M}_{WF}\dfrac{\partial^2 w_W^X|_C}{\partial t^2} - \mathcal{C}_{WF}\dfrac{\partial w_W^X|_C}{\partial t} \\ \tau_{WF} = -\mathcal{I}_{WF}\dfrac{\partial^2 \theta_W^X|_C}{\partial t^2} - \mathcal{C}_{\theta WF}\dfrac{\partial \theta_W^X|_C}{\partial t} \end{cases} \tag{10}$$

where $w_W^X|_C$ denotes the displacement of the wing's geometric center with respect to the inertial frame, and $\mathcal{M}_{WF}$ and $\mathcal{C}_{WF}$ are the fluid-induced added mass and damping per unit length, respectively.

The AVL program is used to obtain the aerodynamic coefficients and stability derivatives assuming the flight speed is low, yielding a low Mach number. The AVL program was developed by Mark Drela from MIT's Department of Aeronautics and Astronautics, and by Harold Youngren from Aerocraft, Inc. AVL is mainly based on an extended vortex lattice method (VLM.) In VLM, the lifting surface is discretized into multiple (N) panels with an idealized zero thickness. Each panel has a horseshoe vortex attached to it. Suppose the flight speed is low, yielding a low Mach number – ignoring the vorticity and viscosity, and using the potential flow theory, the flow velocity is calculated by the vortex strengths [39]. Applying Neumann boundary condition (the velocity normal to the panel is zero) at each collocation point gives the $N \times N$ matrix form vortex equation, where the N vortex strengths are solved. The

extended Theodorsen formulation is used to calculate the unsteady aerodynamic forces [11], where the leading edge vortex contribution is captured by utilizing the static lift curve. In this paper, only the unsteady aerodynamic forces in the Theodorsen formulation are used. The added mass and steady aerodynamic forces are replaced by the models mentioned above.

3.3 Piezoelectric Circuit Domain

Figure 2 shows an R-L-C driving circuit connected to a piezocomposite wing. The piezocomposite wing is represented by a transformer model [40]. The C_p is the internal capacitance of the piezoelectric actuator. A resistor R_p in parallel with the capacitor C_p is used to represent the dielectric leakage. The electromechanical coupling is depicted by the transformer, where the turns ratios are the force-to-voltage ratios, and i_p is the piezoelectric polarization current due to the wing deformation. The inductor (L_C) and capacitor (C_C) are connected in series to magnify the voltage.

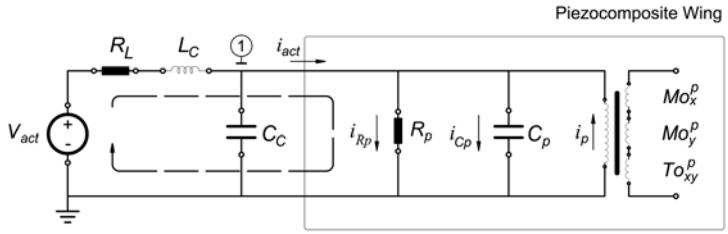

Figure 2: RLC circuit to drive the piezoelectric actuator and the transformer model. The C_C can be adjusted to change the natural frequency.

Piezoelectric materials have direct and converse piezoelectric effects, which refer to charge generation when deformed or straining when exposed to an external electric field [41]. The direct and converse piezoelectric effects cause energy exchange between the morphing wings and the driving circuit. The potential distribution in the MFC device was solved by Sharghi and Bilgen [42], which is used in electromechanical model in this paper.

4 RESULTS

The static ornithopter and wing responses are presented in **Figure 3** (**a**) and (**b**), respectively. Positive DC voltages (1500 V) are applied to the wing, which lead to a static downstroke. A twist is also induced. The lumped-parameter model is computationally economic, which takes seconds on a PC (4 cores of Intel(R) Xeon(R) W-2102 CPU @ 2.90 GHz, 16 GB RAM) for each run.

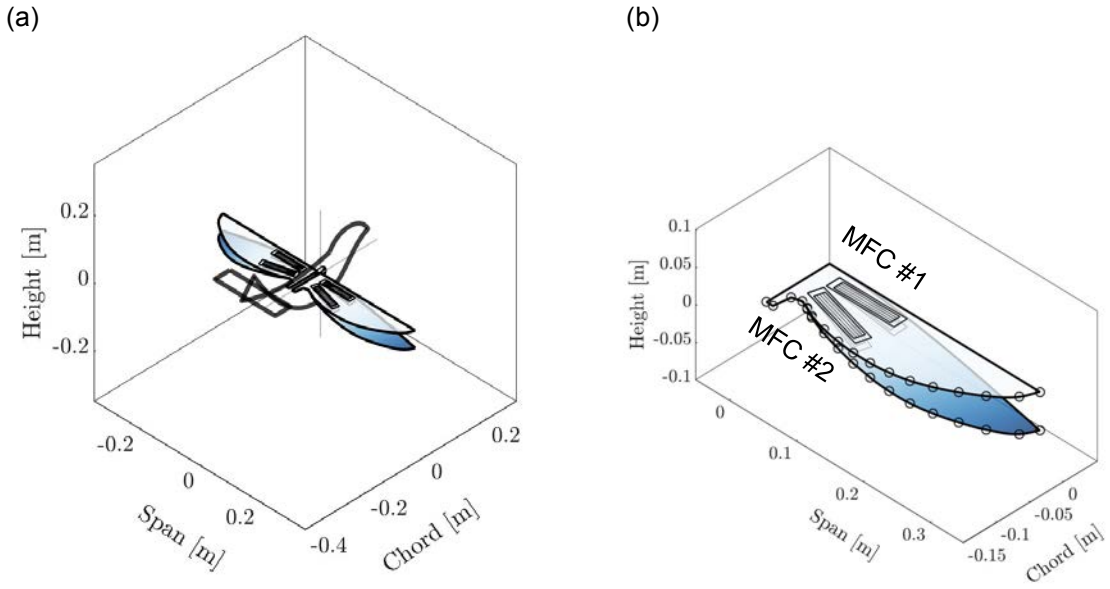

Figure 3: System and wing diagrams. (**a**) ornithopter static response. (**b**) wing static response. The transparent undeformed wing shapes are presented as references. The wing profile and MFC placement in (**b**) are customizable in the Raleigh-Ritz formulation.

Figure 4 (**a**) and (**b**) show the magnitudes of wing tip heave displacement and pitch at maximum chord, as a function of MFC excitation frequency and MFC #2 orientation. The resonance frequency is around 5 Hz, which agrees well with previous experimental observations [14]. A large MFC #2 orientation deviation from the span axis favors the pitch magnitude, as the deviation of MFC introduces twist strain to the wing.

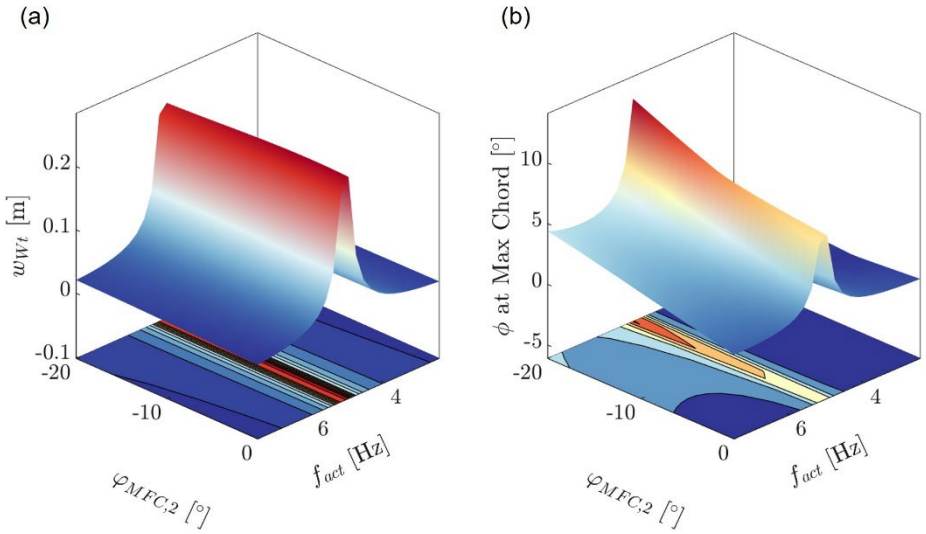

Figure 4: (**a**) wing tip heave displacement and (**b**) pitch responses as a function of excitation frequency and **MFC #2** orientation.

5 CONCLUSIONS

A computationally efficient multi-physics model is presented in this research, which can predict the kinematic, dynamic, and aerodynamic performance of induced-strain actuated mechanism-free ornithopters. The resonance frequency predicted by the model agrees with previous experimental observations. This model can be used in design optimization and real-time control. In the future, wind tunnel experiments will be conducted to tune the unknown coefficients of the model and further improve the accuracy of the model.

ACKNOWLEDGMENTS

The authors acknowledge the support of Rutgers University College of Engineering, and Rutgers University Research Council Award.

REFERENCES

[1] F. Hauris, "Achieving Wing-like Structural Response with Piezocomposite Unimorph Thin Plates," Old Dominion University, 2015.

[2] F. C. Hauris and O. Bilgen, "Induced strain actuation for solid-state ornithopters: A geometric configuration study," in *24th AIAA/AHS Adaptive Structures Conference*, 2016, p. 0818.

[3] F. Hauris and O. Bilgen, "Induced strain actuation for solid-state ornithopters: A parametric study," in *ASME 2014 Conference on Smart Materials, Adaptive Structures and Intelligent Systems*, 2014: American Society of Mechanical Engineers Digital Collection.

[4] J. W. Gerdes, S. K. Gupta, and S. A. Wilkerson, "A review of bird-inspired flapping wing miniature air vehicle designs," *Journal of Mechanisms and Robotics,* 2012.

[5] V. Malolan, M. Dineshkumar, and V. Baskar, "Design and development of flapping wing micro air vehicle," in *42nd AIAA aerospace sciences meeting and exhibit*, 2004, p. 40.

[6] T. N. Pornsin-Sirirak, Y.-C. Tai, C.-M. Ho, and M. Keennon, "Microbat: A palm-sized electrically powered ornithopter," in *Proceedings of NASA/JPL workshop on biomorphic robotics*, 2001, vol. 14: Citeseer.

[7] G. De Croon, M. Perçin, B. Remes, R. Ruijsink, and C. De Wagter, "The delfly," *Dordrecht: Springer Netherlands. doi,* vol. 10, pp. 978-94, 2016.

[8] R. Madangopal, Z. A. Khan, and S. K. Agrawal, "Biologically inspired design of small flapping wing air vehicles using four-bar mechanisms and quasi-steady aerodynamics," *Journal of Mechanical Design,* 2005.

[9] S. K. Banala and S. K. Agrawal, "Design and optimization of a mechanism for out-of-plane insect winglike motion with twist," *Journal of Mechanical Design,* 2005.

[10] M. A. Fenelon and T. Furukawa, "Design of an active flapping wing mechanism and a micro aerial vehicle using a rotary actuator," *Mechanism and Machine Theory,* vol. 45, no. 2, pp. 137-146, 2010.

[11] H. E. Taha, M. R. Hajj, and P. S. Beran, "State-space representation of the unsteady aerodynamics of flapping flight," *Aerospace Science and Technology,* vol. 34, pp. 1-11, 2014.
[12] F. Hauris and O. Bilgen, "Induced Strain Actuation for Solid-State Ornithopters: An Aeroelastic Study," in *Smart Materials, Adaptive Structures and Intelligent Systems*, 2018, vol. 51944: American Society of Mechanical Engineers, p. V001T04A008.
[13] F. Hauris and O. Bilgen, "Induced strain actuation for solid-state ornithopters: pitch and heave coupling," in *Smart Materials, Adaptive Structures and Intelligent Systems*, 2017, vol. 58264: American Society of Mechanical Engineers, p. V002T04A006.
[14] F. Hauris and O. Bilgen, "Parametric modal analysis of an induced-strain actuated wing-like plate for pitch and heave coupling response," *Journal of Intelligent Material Systems and Structures,* vol. 31, no. 15, pp. 1793-1807, 2020.
[15] R. Dudley, *The biomechanics of insect flight: form, function, evolution*. Princeton University Press, 2002.
[16] E. Farrell Helbling and R. J. Wood, "A review of propulsion, power, and control architectures for insect-scale flapping-wing vehicles," *Applied Mechanics Reviews,* vol. 70, no. 1, 2018.
[17] R. S. Fearing, K. H. Chiang, M. H. Dickinson, D. Pick, M. Sitti, and J. Yan, "Wing transmission for a micromechanical flying insect," in *Proceedings 2000 ICRA. Millennium Conference. IEEE International Conference on Robotics and Automation. Symposia Proceedings (Cat. No. 00CH37065)*, 2000, vol. 2: IEEE, pp. 1509-1516.
[18] E. Steltz, S. Avadhanula, and R. S. Fearing, "High lift force with 275 Hz wing beat in MFI," in *2007 IEEE/RSJ International Conference on Intelligent Robots and Systems*, 2007: IEEE, pp. 3987-3992.
[19] R. J. Wood, S. Avadhanula, R. Sahai, E. Steltz, and R. S. Fearing, "Microrobot design using fiber reinforced composites," *Journal of Mechanical Design,* 2008.
[20] S. M. Nogar, A. Gogulapati, J. J. McNamara, A. Serrani, M. W. Oppenheimer, and D. B. Doman, "Control-oriented modeling of coupled electromechanical-aeroelastic dynamics for flapping-wing vehicles," *Journal of Guidance, Control, and Dynamics,* vol. 40, no. 7, pp. 1664-1679, 2017.
[21] J. J. Hollkamp and R. W. Gordon, "Reduced-order models for nonlinear response prediction: Implicit condensation and expansion," *Journal of Sound and Vibration,* vol. 318, no. 4-5, pp. 1139-1153, 2008.
[22] M. McEwan, J. R. Wright, J. E. Cooper, and A. Y. T. Leung, "A combined modal/finite element analysis technique for the dynamic response of a non-linear beam to harmonic excitation," *Journal of Sound and Vibration,* vol. 243, no. 4, pp. 601-624, 2001.
[23] S. Guo, D. Li, and J. Wu, "Theoretical and experimental study of a piezoelectric flapping wing rotor for micro aerial vehicle," *Aerospace Science and Technology,* vol. 23, no. 1, pp. 429-438, 2012.
[24] W. K. Wilkie *et al.*, "Low-cost piezocomposite actuator for structural control applications," 2000, vol. 3991: International Society for Optics and Photonics, pp. 323-335.

[25] J. W. High and W. K. Wilkie, "Method of fabricating NASA-standard macro-fiber composite piezoelectric actuators," 2003.
[26] O. Bilgen, Y. Wang, and D. J. Inman, "Electromechanical comparison of cantilevered beams with multifunctional piezoceramic devices," *Mechanical Systems and Signal Processing,* vol. 27, pp. 763-777, 2012.
[27] O. Bilgen, "Aerodynamic and electromechanical design, modeling and implementation of piezocomposite airfoils," Virginia Tech, 2010.
[28] X. Shan and O. Bilgen, "A reduced-order multi-body model with electromechanical-aeroelastic coupling for mechanism-free ornithopters," *Journal of Fluids and Structures,* vol. 114, p. 103724, 2022.
[29] X. Shan and O. Bilgen, "A lumped-parameter coupled electro-piezo-aeroelastic model for flapping wings," *International Journal of Mechanical Sciences,* vol. 234, p. 107690, 2022.
[30] M. Katibeh and O. Bilgen, "Design Optimization of a Piezocomposite Ornithopter Wing Planform Using a Genetic Algorithm," in *Smart Materials, Adaptive Structures and Intelligent Systems*, 2022, vol. 86274: American Society of Mechanical Engineers, p. V001T04A008.
[31] M. Katibeh and O. Bilgen, "An Experimental and Numerical Study of a Solid-State Ornithopter Wing Performance," in *Smart Materials, Adaptive Structures and Intelligent Systems*, 2021, vol. 85499: American Society of Mechanical Engineers, p. V001T05A007.
[32] M. Katibeh and O. Bilgen, "Parametric Analysis of Structural Properties of a Rectangular Partially-Clamped Wing," in *Smart Materials, Adaptive Structures and Intelligent Systems*, 2020, vol. 84027: American Society of Mechanical Engineers, p. V001T04A006.
[33] M. Katibeh and O. Bilgen, "Transient fluid-structure interaction analysis of a solid state ornithopter wing," in *Smart Materials, Adaptive Structures and Intelligent Systems*, 2019, vol. 59131: American Society of Mechanical Engineers, p. V001T04A005.
[34] E. F. Crawley and K. B. Lazarus, "Induced strain actuation of isotropic and anisotropic plates," *AIAA journal,* vol. 29, no. 6, pp. 944-951, 1991.
[35] T. Theodorsen, "General theory of aerodynamic instability and the mechanism of flutter. NACA," TR 496, 1935.
[36] J. N. Reddy, *Theory and analysis of elastic plates and shells*. CRC press, 2006.
[37] M. Aureli, M. Basaran, and M. Porfiri, "Nonlinear finite amplitude vibrations of sharp-edged beams in viscous fluids," *Journal of Sound and Vibration,* vol. 331, no. 7, pp. 1624-1654, 2012.
[38] T. Naik, E. K. Longmire, and S. C. Mantell, "Dynamic response of a cantilever in liquid near a solid wall," *Sensors and Actuators A: Physical,* vol. 102, no. 3, pp. 240-254, 2003/01/01/ 2003.
[39] M. Drela, *Flight vehicle aerodynamics*. MIT press, 2014.
[40] S. Roundy and P. K. Wright, "A piezoelectric vibration based generator for wireless electronics," *Smart Materials and structures,* vol. 13, no. 5, p. 1131, 2004.

[41] F. Standards Committee of the IEEE Ultrasonics and F. C. Society, "IEEE Standard on Piezoelectricity," ed: IEEE New York, 1987.
[42] H. Sharghi and O. Bilgen, "Continuous electric field modeling of Macro-Fiber Composites for actuation and energy harvesting," *International Journal of Mechanical Sciences,* vol. 213, p. 106864, 2022.